Coupled guided modes in the magnetotails: spatial structure and ballooning instability

A. S. Leonovich & D. A. Kozlov

Astrophysics and Space Science
An International Journal of Astronomy, Astrophysics and Space Science

ISSN 0004-640X
Volume 353
Number 1

Astrophys Space Sci (2014) 353:9-23
DOI 10.1007/s10509-014-1999-3

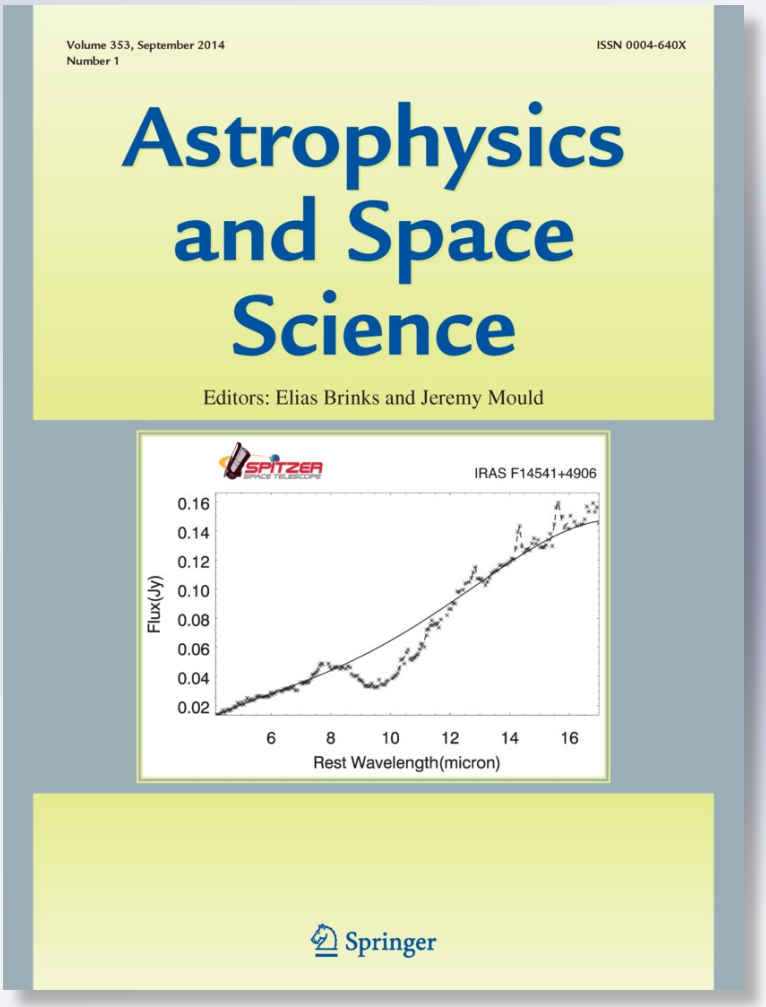

Springer

Astrophys Space Sci (2014) 353:9–23
DOI 10.1007/s10509-014-1999-3

ORIGINAL ARTICLE

Coupled guided modes in the magnetotails: spatial structure and ballooning instability

A.S. Leonovich · D.A. Kozlov

Received: 29 April 2014 / Accepted: 1 June 2014 / Published online: 7 June 2014

Abstract The problem of the spatial structure of coupled azimuthally small-scale Alfvén and slow magnetosonic (SMS) waves is solved in an axisymmetric magnetotail model with a current sheet. It is shown that the linear transformation of these waves occurs in the current sheet on magnetic field lines stretched into the magnetotail. From the ionosphere to the current sheet these modes are linearly independent. Due to the high ionospheric conductivity the structure of coupled modes along magnetic field lines represents standing waves with very different typical scales in different parts of the field line. In most of the field line their structure is determined by the large-scale Alfvén wave structure. Near the ionosphere and in the current sheet, small-scale SMS wave field starts to dominate. In these regions coupled modes becomes small-scale. Such modes are neutrally stable on the field lines that do not cross the current sheet, but switch to the ballooning instability regime on field lines crossing the current sheet. An external source is required to generate these modes and this paper considers external currents in the ionosphere as a possible driver. In the direction across magnetic shells the coupled modes are waves running away from the magnetic shell on which they were generated.

Keywords MHD-oscillations · Coupled modes · Magnetotail · Ballooning instability

A.S. Leonovich (✉) · D.A. Kozlov
Institute of Solar-Terrestrial Physics SB RAS, P.O. Box 291, Irkutsk 664033, Russia
e-mail: leon@iszf.irk.ru

1 Introduction

A common feature in the magnetospheres of planets having their own magnetic field are magnetotails formed under interaction with the solar wind flow (Blanc et al. 2005; Kivelson 2007). Most magnetotails have a current sheet dividing it into two lobes (for example, the geotail). The current is closed through the magnetopause forming a magnetic field, which is almost dipole near Earth, and exhibits a small curvature radius at the top of field lines stretched into the magnetotail. This creates specific conditions for the propagation of and interaction between the Alfvén and slow magnetosonic (SMS) waves.

Ultra-low-frequency (ULF) MHD oscillations can be generated by various sources in the magnetosphere, for example, under the impact of shock waves propagating in the solar wind on the magnetopause (Guglielmi et al. 2000; Kangas et al. 2001). Fast magnetosonic (FMS) waves can either penetrate into the magnetosphere from the solar wind (Leonovich et al. 2003) or be generated by the Kelvin–Helmholtz instability when the solar wind flows around the magnetopause (McKenzie 1970; Mazur and Chuiko 2011; Leonovich 2011). It is known that the direction of FMS waves propagation is defined by their spatial structure and can take any direction with respect to the background magnetic field. Phase velocity direction for Alfvén and SMS waves is close to the background magnetic field, which creates an opportunity for their being "confined" on magnetic shells bounded by the highly conductive ionosphere of Earth's magneto-conjugated hemispheres. Therefore these waves form a structure comprising a set of standing waves along the geomagnetic field lines.

In a plasma that is inhomogeneous across magnetic field lines, FMS waves can drive resonant Alfvén waves—the so-called field line resonance (Tamao 1965; Southwood 1974;

Chen and Hasegawa 1974)—or SMS-waves—the magnetosonic resonance (Yumoto 1985; Klimushkin et al. 2010; Leonovich and Kozlov 2013a). Resonant interaction also takes place in a plasma that is inhomogeneous not only across magnetic shells but along magnetic field lines as well. This resonance occurs for both monochromatic (Rankin et al. 2000; Leonovich 2001) and broadband MHD oscillations (Leonovich and Mazur 1989; Lee and Lysak 1999; Agapitov et al. 2009; Dmitrienko 2013). If the plasma configuration under study is axisymmetric the MHD-wave field can be decomposed into the sum of the azimuthal harmonics of the form $\exp(im\phi)$, where ϕ is the azimuthal angle, $m = 0, 1, 2, \ldots$ is the azimuthal wave number. Resonant interaction is most effective for the $m \sim 1$ harmonics. For $m = 0$, any coupling is absent between the harmonics of Alfvén and FMS waves, in the ideal MHD approximation. In terms of two-fluid MHD, however, and with plasma ion gyrotropy taken into account, field line resonance exists even for $m = 0$ harmonics (Leonovich et al. 1983).

The situation is completely different for MHD waves with $m \gg 1$. Such FMS waves fail to penetrate from the solar wind into the magnetosphere, with a sufficiently large amplitude, because the magnetosphere is an opacity region for them. Therefore, the source for guided waves (Alfvén and SMS waves) should be located on the same magnetic shells where these waves are confined. For example, these waves can be generated in the magnetosphere by external currents in the ionosphere (Leonovich and Mazur 1993). On the field lines stretched into the magnetotail these modes can interact creating a complex wave-field pattern (Southwood and Saunders 1985; Walker 1987; Cheremnykh and Parnowski 2006). These oscillations can go into the ballooning instability regime in the current sheet (Ohtani et al. 1989; Hameiri et al. 1991; Liu 1997)

Often the simplest approximation is used for examining the ballooning instability, in which the local dispersion equation is analyzed (Liu 1997; Mazur et al. 2012; Klimushkin et al. 2012). This equation is derived for a medium that is homogeneous along the magnetic field lines that have identical parameters to the current sheet. As was shown in Leonovich and Kozlov (2013b), however, solutions of MHD equations obtained for the same geotail model give different results in the local approach and a WKB approximation taking into account variations of the medium parameters along magnetic field lines.

First and foremost, it should be noted that there are two unrelated branches of MHD oscillations in each of these approximations—the Alfvén and SMS waves. Solutions obtained in the local approximation show that, under certain conditions, SMS-wave transfer to the aperiodic ballooning instability regime and Alfvén wave remains stable under any medium parameters. In contrast, solutions obtained in the WKB approximation show that both SMS and Alfvén oscillations can transfer to the ballooning instability regime with non-zero frequency on the field lines passing through the current sheet. Since the WKB approximation takes into account the full structure of the oscillations along the field line, the results obtained in the local approximation are apparently not applicable to the analysis of MHD oscillations in real, strongly inhomogeneous, plasma configurations such as magnetic tails of planetary magnetospheres.

Solutions were analyzed in Leonovich and Kozlov (2013b) for the basic and the first few harmonics of the waves standing between the magnetoconjugated ionospheres. However, the WKB approximation over the longitudinal coordinate used there, being better than the local approximation, is still poorly applicable to the basic harmonics of oscillations with wavelengths comparable to the magnetospheric plasma inhomogeneity scale. Therefore, this paper carries out a numerical solution of the equation describing the Alfvén and SMS waves for axisymmetric geotail model in Leonovich and Kozlov (2013b). This will not only allow the results obtained earlier in the WKB approximation to be verified, but also the spatial field distribution of the coupled Alfvén and SMS waves to be calculated, which cannot be done in the WKB approximation. Besides, we will carry out an analytical study of the Alfvén and SMS oscillation coupling conditions in the current sheet. In this paper we restrict ourselves to calculating the field of the basic (even) harmonic and the second (odd) harmonic of standing waves for the coupled modes.

The structure of this paper is as follow. Section 2 presents the axisymmetric model involved for the geotail with current sheet and the basic equation describing the spatial structure of the coupled guided modes. In Sect. 3 the problem is numerically solved of the structure of coupled modes along geomagnetic field lines. A qualitative analytical study of a linear transformation of the Alfvén and SMS waves in the vicinity of the singular points of the equation describing the structure of the coupled modes along the magnetic field lines is contained in Sect. 4. In Sect. 5 we solve the problem of the oscillation structure across magnetic shells. The main results of the work are listed in the Conclusion.

2 Medium model and governing equation

Let us introduce an orthogonal curvilinear coordinate system (x^1, x^2, x^3) tied to magnetic field lines (see Fig. 1). The x^3 coordinate is directed along the field line, the x^1 coordinate is across magnetic shells, and the x^2 coordinate is such that the system should be a right-side system. Let us model a magnetic field with tailward-stretched closed field lines as the sum of a dipole magnetic field and the magnetic field of an azimuthal current localized near the equatorial plane. In order to describe the MHD oscillations we will use the set of ideal MHD equations:

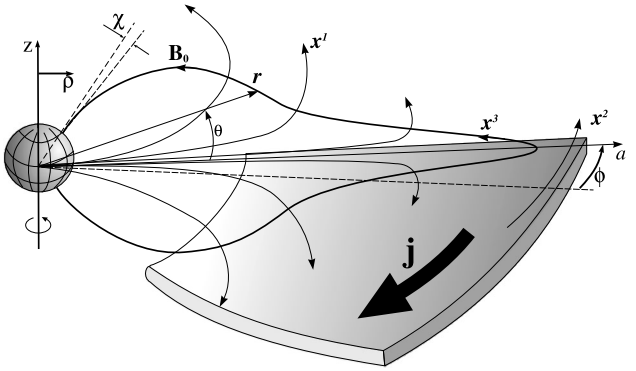

Fig. 1 An axisymmetric model of the geomagnetic tail with a current sheet. The coordinate systems used: the orthogonal (x^1, x^2, x^3) and non-orthogonal (a, ϕ, θ) curvilinear system tied to the magnetic field lines, the cylindrical system (ρ, ϕ, z)

$$\rho \frac{d\bar{\mathbf{v}}}{dt} = -\nabla \bar{P} + \frac{1}{4\pi}[\mathrm{curl}\,\bar{\mathbf{B}} \times \bar{\mathbf{B}}], \tag{1}$$

$$\frac{\partial \bar{\mathbf{B}}}{\partial t} = \mathrm{curl}[\bar{\mathbf{v}} \times \bar{\mathbf{B}}], \tag{2}$$

$$\frac{\partial \bar{\rho}}{\partial t} + \nabla(\rho \bar{\mathbf{v}}) = 0, \tag{3}$$

$$\frac{d}{dt}\frac{\bar{P}}{\bar{\rho}^{\gamma}} = 0, \tag{4}$$

where $\bar{\mathbf{B}}$ and $\bar{\mathbf{v}}$ are the magnetic field and plasma velocity vectors, $\bar{\rho}$ and $\bar{P}$ are the plasma density and pressure, and $\gamma = 5/3$ is the adiabatic index. We restrict ourselves to small-amplitude perturbations. This allows us to linearize the system (1)–(4). The parameters of unperturbed plasma will be subscripted with '0', while leaving the perturbed parameters unindexed ($\bar{\rho} = \rho_0 + \rho$, $\bar{P} = P_0 + P$, $\bar{\mathbf{B}} = \mathbf{B}_0 + \mathbf{B}$, $\bar{\mathbf{v}} = \mathbf{v}_0 + \mathbf{v}$). Unperturbed plasma is assumed to be stationary ($\mathbf{v}_0 = 0$). To the leading order of the perturbation theory, (1) yields the equilibrium condition for a plasma configuration

$$\nabla P_0 = \frac{1}{4\pi}[\mathrm{curl}\,\mathbf{B_0} \times \mathbf{B_0}]. \tag{5}$$

Let us also use the frozen-in condition linking the electric field and velocity vectors:

$$\mathbf{E} = -[\mathbf{v} \times \mathbf{B}_0]/c. \tag{6}$$

In this approximation, perturbed electric field is perpendicular to the background magnetic field.

An axisymmetric model of the geomagnetic tail is presented in Appendix A. Figure 2 depicts magnetic field lines in a model of the geotail with the current sheet calculated with (34) and distributions of the Alfvén speed $A = B_0/\sqrt{4\pi\rho_0}$ (Fig. 2a) and SMS wave speed $C_s = AS/\sqrt{A^2 + S^2}$ (where $S = \sqrt{\gamma P_0/\rho_0}$ is sound speed in plasma) in the meridional plane (Fig. 2b).

Let us construct an equation describing a spatial structure of monochromatic MHD waves with large azimuthal wave

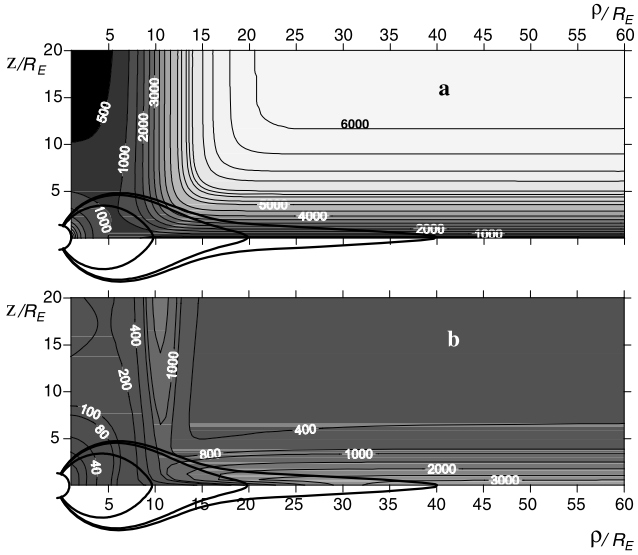

Fig. 2 The distribution of (**a**) Alfvén speed A (km/s) and (**b**) SMS speed C_S (km/s) in the meridional plane calculated using the model geotail with a current sheet

numbers ($m \gg 1$). In accordance with Helmholtz's expansion theorem, an arbitrary vector field whose first derivatives are defined at each point can be resolved as the sum of the potential and solenoidal vector fields (Korn and Korn 1968). For an electric field lacking the longitudinal component, the decomposition takes the form

$$\mathbf{E} = -\nabla_{\perp}\varphi + [\boldsymbol{\nabla}_{\perp} \times \boldsymbol{\Psi}], \tag{7}$$

where $\boldsymbol{\nabla}_{\perp}$ is the gradient across magnetic field lines, φ and $\boldsymbol{\Psi}$ are, respectively, the scalar and vector potential of the perturbed electric field. With certain gauge, the vector potential can be chosen such as to have the longitudinal component only, $\boldsymbol{\Psi} = (0, 0, \psi)$.

In an axisymmetric medium model, the solutions to the linearized system (1)–(4) can be sought as a Fourier decomposition into harmonics $\exp(ik_2x^2 - i\omega t)$, where k_2 is the azimuthal component of the wave vector (if $x^2 \equiv \phi$, where ϕ is the azimuthal angle, $k_2 = m = 0, 1, 2, 3, \ldots$ is the azimuthal wave number), ω is the wave frequency. Let us consider oscillations with large azimuthal wave numbers $m \gg 1$. The equation for a scalar potential of such oscillations was derived in Leonovich and Kozlov (2013b):

$$\widehat{L}_S \nabla_1 \widehat{L}_T \nabla_1 \varphi - k_2^2(\widehat{L}_S \widehat{L}_P + \widehat{L}_C)\varphi = 0, \tag{8}$$

where $\nabla_i \equiv \partial/\partial x^i$ and the following operators in the longitudinal x^3 coordinate are introduced:

$$\widehat{L}_T = \frac{1}{\sqrt{g_3}}\nabla_3 \frac{p}{\sqrt{g_3}}\nabla_3 + p\frac{\omega^2}{A^2},$$

$$\widehat{L}_P = \frac{1}{\sqrt{g_3}}\nabla_3 \frac{p^{-1}}{\sqrt{g_3}}\nabla_3 + p^{-1}\frac{\omega^2}{A^2},$$

which are the longitudinal toroidal and poloidal operators describing the structure of Alfvén oscillations with toroidal

($m = 0$) and poloidal ($m \to \infty$) polarization in a "cold plasma", $p = \sqrt{g_2/g_1}$, where $g_{1,2,3}$ are the metric tensor components,

$$\widehat{L}_S = \frac{\varkappa_{1g}\rho_0}{B_0 P_0^\sigma \sqrt{g}} \nabla_3 \frac{\sqrt{g}}{g_3} \frac{P_0^\sigma}{\rho_0} \nabla_3 \frac{B_0}{\varkappa_{1g}} + \frac{\omega^2}{C_s^2},$$

$$\widehat{L}_C = \frac{\varkappa_{1g}\omega^2}{A^2\sqrt{g_1 g_2}} \left[\frac{B_0}{\omega^2 P_0^\sigma \sqrt{g_3}} \nabla_3 \frac{\varkappa_{1B} A^2 P_0^\sigma}{B_0 \sqrt{g_3}} \nabla_3 - \varkappa_{1P} \right],$$

where

$$\varkappa_{1g} = \nabla_1(\ln\sqrt{g_3}), \qquad \varkappa_{1B} = \nabla_1(\ln\sqrt{g_3}B_0), \\ \varkappa_{1P} = \nabla_1\left(\ln\sqrt{g_3}P_0^\sigma/B_0\right), \tag{9}$$

$g = \sqrt{g_1 g_2 g_3}$, $\sigma = 1/\gamma$. The relation between potentials φ and ψ for MHD oscillations with $m \gg 1$ takes the form:

$$ik_2 B_0 \frac{\varkappa_{1g}}{\sqrt{g_3}} \widetilde{\Delta}_\perp \psi \approx \nabla_1 B_0 \widehat{L}_T \nabla_1 \varphi - k_2^2 B_0 \widehat{L}_P \varphi, \tag{10}$$

where

$$\widetilde{\Delta}_\perp = \frac{g_3}{\sqrt{g}} \nabla_1 \frac{g_2}{\sqrt{g}} \nabla_1 - \frac{k_2^2}{g_2}.$$

Let us express the components of the oscillation field in terms of potentials φ and ψ. We get from (7):

$$E_1 = -\nabla_1\varphi + ik_2 \frac{g_1}{\sqrt{g}}\psi,$$

$$E_2 = -ik_2\varphi - \frac{g_2}{\sqrt{g}}\nabla_1\psi,$$

$$E_3 = 0.$$

Using (11), (2) and (6), we can obtain the following expressions for components of a perturbed magnetic field and velocity:

$$B_1 = \frac{c}{\omega}\frac{g_1}{\sqrt{g}}\nabla_3\left(k_2\varphi - i\frac{g_2}{\sqrt{g}}\nabla_1\psi\right),$$

$$B_2 = \frac{c}{\omega}\frac{g_2}{\sqrt{g}}\nabla_3\left(i\nabla_1\varphi + k_2\frac{g_1}{\sqrt{g}}\psi\right),$$

$$B_3 = i\frac{c}{\omega}\widetilde{\Delta}_\perp\psi,$$

$$v_1 = -\frac{cp^{-1}}{B_0}\left(ik_2\varphi + \frac{g_2}{\sqrt{g}}\nabla_1\psi\right),$$

$$v_2 = \frac{cp}{B_0}\left(\nabla_1\varphi - ik_2\frac{g_1}{\sqrt{g}}\psi\right).$$

The perturbed pressure and the v_3 component of the velocity are described by two coupled equations. The first one can be obtained from the third component of a linearized equation (1)

$$v_3 = -\frac{i}{\omega\rho_0}\nabla_3 P + \frac{icB_0\varkappa_{1B}}{4\pi\rho_0\omega^2\sqrt{g_1 g_2}}\left(k_2\varphi - i\frac{g_2}{\sqrt{g}}\nabla_1\psi\right),$$

and we have the second equation from linearized equations (3) and (4):

$$P = -i\frac{S^2\rho_0}{\omega P_0^\sigma\sqrt{g}}\left[\nabla_1\left(\frac{\sqrt{g}}{g_1}P_0^\sigma v_1\right) + ik_2\frac{\sqrt{g}}{g_2}P_0^\sigma v_2 + \nabla_3\left(\frac{\sqrt{g}}{g_3}P_0^\sigma v_3\right)\right].$$

Equation (8) describes the structure of azimuthally small-scale MHD oscillations in the meridional plane. This equation should be complemented with boundary conditions at the ends of closed field lines that intersect the ionosphere in the Northern ($x^3 = x_+^3$) and Southern ($x^3 = x_-^3$) hemispheres. The ionosphere is a highly conductive medium. With external currents flowing in the ionosphere, the boundary conditions for the potential φ (Leonovich and Mazur 1996) are

$$\varphi(l_\pm) = \mp i\frac{v_\pm}{\omega}\frac{\partial\varphi}{\partial l}\bigg|_{l_\pm} - \frac{J_\parallel^\pm}{V_\pm}, \tag{11}$$

where $dl = \sqrt{g_3}dx^3$ is the length element along the field line, the $\pm$ signs correspond to the parameters in the Northern ($+$) and Southern ($-$) hemispheres, $v_\pm = c^2\cos\chi_\pm/4\pi\Sigma_{P\pm}$, $V_\pm = \Sigma_{P\pm}/\cos\chi_\pm$, where $\Sigma_{P_\pm}$ is Pedersen conductivity of the ionosphere, $\chi_\pm$ is the angle between the field line and the normal to the ionosphere (see Fig. 1), and the function $J_\parallel^\pm$ is related to the density of field-aligned currents in the ionosphere $j_\parallel^\pm$ by

$$\Delta_\perp J_\parallel^\pm = j_\parallel^\pm.$$

The relation of field-aligned currents $j_\parallel$ to wave processes in the ionosphere is defined in Appendix A. The solutions of (8) with the boundary conditions (11) were found in the WKB approximation over the x^3 coordinate in Leonovich and Kozlov (2013b). In this paper we will seek the numerical solutions of (8) for the fundamental and second harmonics of standing Alfvén waves as well as analytically investigating the mechanism of their coupling with SMS waves in the current sheet. Lower-frequency SMS oscillations will not be considered here for they are strongly dissipative modes and are more difficult to drive in the magnetosphere than the Alfvén waves.

3 The structure of coupled Alfvén and SMS waves along magnetic field lines

As was shown in Kozlov et al. (2006), Alfvén oscillations with $m \gg 1$ can be driven in the vicinity of the poloidal resonant shell by external ionospheric currents whose spectrum includes the eigenfrequencies of standing poloidal Alfvén waves. Another source of such Alfvén oscillations are the flows of high energetic particles in the magnetosphere (Mager and Klimushkin 2005). If we describe the structure of the oscillations in hand in the WKB approximation over the x^1 coordinate as $\varphi \sim \exp(i\int k_1(x^1)dx^1)$,

the relation $|k_1/k_2| \to 0$ is correct in the vicinity of the poloidal resonant shell. The oscillations generated near this shell run across magnetic shells to the toroidal resonant shell (where $|k_1/k_2| \to \infty$), remaining standing waves along magnetic field lines. While traveling from the poloidal to the toroidal resonant shell, the polarization of Alfvén waves changes from poloidal to toroidal. In the vicinity of toroidal resonant shell (the Alfvén resonance region) oscillations are fully absorbed due to ionospheric dissipation. Therefore, there is no wave reflected from the toroidal shell.

As will be shown further, the distance between the poloidal and the toroidal shells is larger in this case than in the case of a "cold plasma". Poloidal oscillations are likely to be absorbed very close to the poloidal resonant shell where they are generated. In order to describe the structure of these oscillations along magnetic field lines in the vicinity of the poloidal resonant shell only the operator proportional to k_2^2 should be left in Eq. (8), in the zeroth approximation:

$$\widehat{L}_S \widehat{L}_P \varphi + \widehat{L}_C \varphi \approx 0. \tag{12}$$

The structure of the fundamental harmonics is such that their typical wave length along geomagnetic field lines is much larger than their wave length in the directions perpendicular to field lines. Using the multiple scale technique, we can seek the structure of oscillations in the meridional plane in the form:

$$\varphi = U\left(x^1\right) H\left(x^1, x^3\right), \tag{13}$$

where $U(x^1)$ describes the small-scale structure of oscillations across magnetic shells, $H(x^1, x^3)$ describes their structure along magnetic field lines (here the dependence on x^1 is defined by varying the coefficients (12) on the inhomogeneity scale).

In the local approach, the dispersion equation can be obtained from (12):

$$\left(\frac{\omega^2}{k_\parallel^2} - A^2\right)\left(\frac{\omega^2}{k_\parallel^2} - c_s^2\right) = \frac{\bar{\varkappa}_{1g} c_s^2}{k_\parallel^2}\left(\frac{\omega^2}{k_\parallel^2}\bar{\varkappa}_{1P} + A^2 \bar{\varkappa}_{1B}\right), \tag{14}$$

where $k_\parallel = k_3/\sqrt{g_3}$, $\bar{\varkappa}_1 = \varkappa_1/\sqrt{g_1}$ are the scaled components of the corresponding parameters. As is shown in Leonovich and Kozlov (2013b), Eq. (14) fully corresponds to the dispersion equations for ballooning modes obtained in Liu (1997), Mazur et al. (2012), Klimushkin et al. (2012).

Substituting (13) into (12) and differentiating the result produces an equation for the $H(x^1, x^3)$ function

$$\left[\nabla_l^4 + \kappa_3 \nabla_l^3 + \kappa_2 \nabla_l^2 + \kappa_1 \nabla_l + \kappa_0\right] H = 0, \tag{15}$$

where $\nabla_l \equiv \partial/\partial l = (g_3)^{-1/2}\nabla_3$ is a derivative with respect to the longitudinal l coordinate, the length element of which, in the coordinate system (a, ϕ, θ), has the form

$$dl = \sqrt{r^2(a,\theta) + (\partial r/\partial\theta)^2}\, d\theta.$$

Radius $r(a, \theta)$ of the point on the field line is defined by (34), and the expressions for the κ_i coefficients are given in Appendix B.

For a numerical integration of Eq. (15) the latter should be supplemented by the boundary conditions on the ionosphere. In the same zero-order approximation, in which Eq. (15) was obtained, we will assume the ionosphere to be perfectly conductive. Therefore, the boundary conditions are reduced to the requirement that the electric field oscillation components tangential to the ionosphere, defined through E_1 and E_2, should tend to zero. It follows from (11) that, when ($|k_1/k_2| \to 0$),

$$\varphi(l_\pm) = 0, \tag{16}$$

where $l_\pm$ are the coordinates of the field line intersection points with the ionospheres of the Northern and Southern hemispheres, respectively. As follows from (10), the boundary condition $\psi(l_\pm) = 0$ implies that $\widehat{L}_P \varphi|_{l_\pm} = 0$ or, given (16),

$$\nabla_l^2 \varphi|_{l_\pm} = \varkappa_{lp} \nabla_l \varphi|_{l_\pm}, \tag{17}$$

where $\varkappa_{lp} = \nabla_l(\ln p^{-1})$. In the numerical integration of (15) the value of $\nabla_l \varphi|_{l_-}$ can be chosen arbitrary as it determines the amplitude of the solution and is defined by normalization. When integrating a fourth-order equation, the first stage should be to specify the third derivative on the ionosphere $\varphi_-''' \equiv \nabla_l^3 \varphi|_{l_-}$ (assuming that the integration starts from the ionosphere of the Southern Hemisphere). $\varphi'''(l_-)$ is not defined from any other boundary conditions. Since on the other end of the field line the required solution must also satisfy to two boundary conditions, (16) and (17), it is determined by two eigenvalues of the parameters of the problem in question.

As such parameters, we choose the eigenfrequency of standing waves between the ionospheres (denoted by $\omega = \Omega_N$, where $N = 1, 2, 3$, is the longitudinal wave number of a large-scale poloidal standing Alfvén wave) and the corresponding value of the third derivative of the required function on the ionosphere $\varphi_{N-}''' \equiv \varphi_N'''(l_-)$. Note that eigenvalue Ω_N should not be seen as the eigen-frequency of the entire problem (8). Both eigenvalues, Ω_N and φ_{N-}''', determine the spatial structure of the harmonic of the standing waves on the magnetic shell at hand. They are functions of the transverse coordinate $\Omega_N \equiv \Omega_N(x^1)$, $\varphi_{N-}''' \equiv \varphi_{N-}'''(x^1)$.

As will be seen from the following calculations, the value of $\mathrm{Re}(\Omega_N(x^1))$ can be thought of as the frequency in the spectrum of the external source capable of driving the N-th harmonic of standing waves on the resonant magnetic shell in question. $\mathrm{Im}(\Omega_N(x^1))$ determines the distribution of the amplitude of these oscillations across magnetic shells.

To simplify our numerical calculations, let us make use of the model symmetry with respect to the equatorial plane. The second pair of boundary conditions can then be formulated for the equatorial plane as follows. For even modes

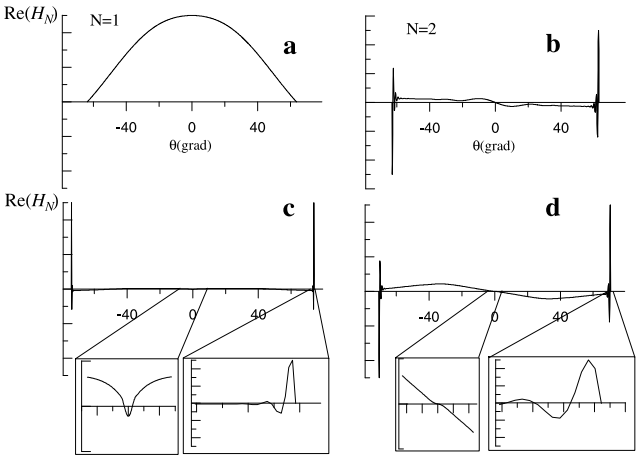

Fig. 3 The longitudinal (along a field line) distribution of the scalar potential of the fundamental ($N = 1$) and second ($N = 2$) harmonics of coupled modes: (**a**) and (**b**) in the inner magnetosphere on the $L = 6$ shell; (**c**) and (**d**) in the current sheet region on the $L = 15$ shell. Here θ is latitude as counted from the equatorial plane (see Fig. 1)

($N = 1, 3, 5, \ldots$ in our notation) this means that all the odd derivatives of the required function are equal to zero. Requirements $\nabla_l \varphi|_{l_e} = \nabla_l^3 \varphi|_{l_e} = 0$, where $l = l_e$ is the equatorial plane coordinate, are enough for our problem. For odd modes ($N = 2, 4, 6, \ldots$) the corresponding boundary conditions have the form $\varphi(l_e) = \nabla_l^2 \varphi|_{l_e} = 0$.

Figure 3 shows the structure of the first two harmonics of standing waves along the magnetic field lines, obtained from the numerical solution of Eq. (15) with the boundary conditions (16), (17) on the ionosphere. The structure of standing waves on magnetic shells, one of which is located in the inner magnetosphere (magnetic shell $L = a/R_E = 6$, where a is the equatorial radius of the field line, R_E is the Earth's radius), are shown in Figs. 3a and 3b, and the second one intersects the current sheet ($L = 15$) in Figs. 3c and 3d. The oscillation parameters in the current sheet (Figs. 3c and 3d) were computed by gradual transformation of the solutions found in the inner magnetosphere (Figs. 3a and 3b) while moving, at a small step, across magnetic shells in the current sheet area.

Of most interest here is the presence of a small-scale structure in the oscillation eigenfunctions near the ionosphere. This is likely to be a manifestation of a small-scale SMS wave coupled with a large-scale Alfvén wave. What is unusual here is that it manifests itself not only in the current layer, as was expected in some previous papers (see Walker and Pekrides 1996; Leonovich and Kozlov 2013b), but near the ionosphere as well. Such a structure have also been obtained in the numerical calculations in Cheremnykh and Parnowski (2006), Parnowski (2007), Mazur et al. (2014), where, however, it appeared only in a few individual components of the oscillation field. According to our calculations, this feature should appear in all components for they all are expressed in terms of the scalar potential φ.

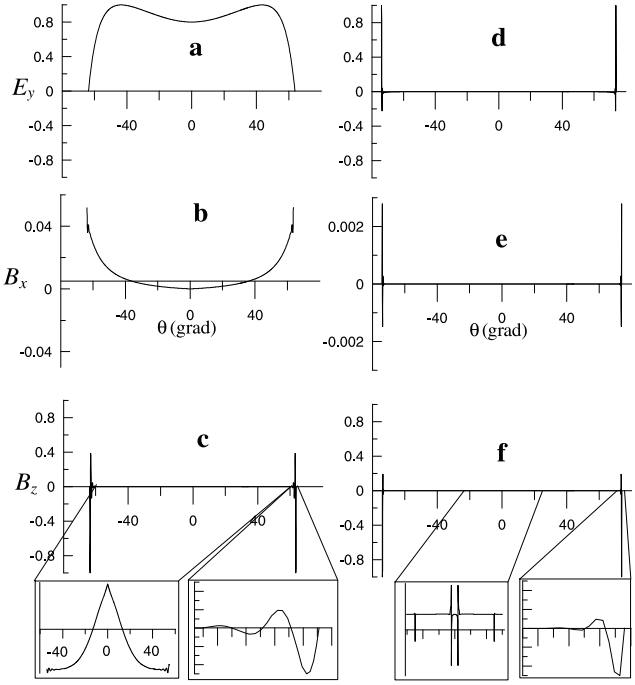

Fig. 4 The longitudinal distribution of the amplitude-normalized leading components of electromagnetic field oscillations (E_y, B_x, B_z) for the fundamental harmonics ($N = 1$) of coupled modes: (**a**), (**b**), and (**c**) in the inner magnetosphere on the $L = 6$ shell; (**d**), (**e**), and (**f**) in the current sheet region on the $L = 15$ shell. *Sharp peaks* in the oscillation field distribution at magnetic field lines crossing the current sheet correspond to the inflection points of the field line. Here θ is latitude as counted from the equatorial plane (see Fig. 1)

Spatial structure refinement for this oscillation is also observed in the current sheet but with smaller amplitude. This is also linked to coupling between a large-scale Alfvén wave and a small-scale SMS wave in the equatorial region, which is particularly intense in the current sheet. It becomes difficult enough to rely on the shape of their large-scale component in determining any link between the oscillation and an initial harmonic of the standing waves on magnetic shells inside the current sheet, due to the small-scale oscillation structure both near the ionosphere, and in the current sheet.

Figure 4 presents the distribution of the main electromagnetic field components E_y, B_x, B_z of the oscillations of interest along magnetic field lines, for the fundamental harmonic $N = 1$, on the same magnetic shells $L = 6$ and $L = 15$. The small-scale constituent near the ionosphere manifests itself even more obviously in these components. This is due to the distribution features of plasma parameters in a magnetic field with field lines converging toward the ionosphere (see Erkaev et al. 2005).

Refinement of the spatial structure of the oscillation field components is more complex in the current sheet. The behavior of the structure of the B_z-component of the field in the equatorial area is shown in the bottom of Fig. 4. Sharp peaks in the structure on field lines crossing the current sheet

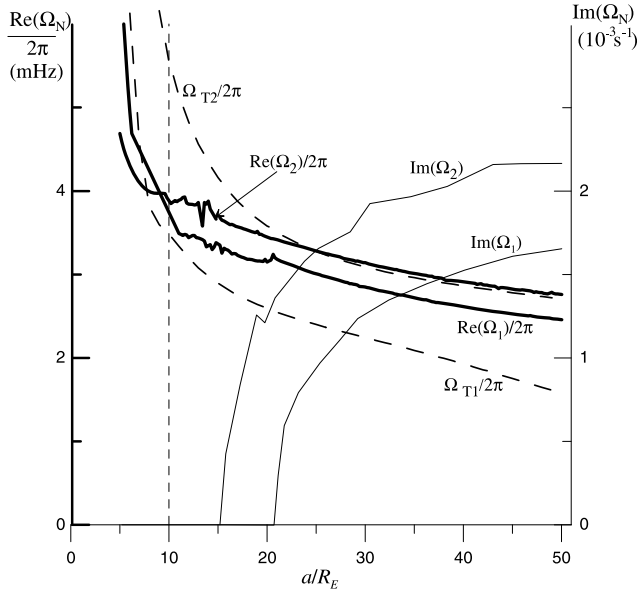

Fig. 5 The transverse (across magnetic shells) distribution of the eigenfrequencies of fundamental ($N = 1$) and second ($N = 2$) harmonics of toroidal (*thick dashed lines*) and coupled modes (*thick solid lines*), their increments in the current sheet region (*thin solid lines*)

are due to the fact that the $\varkappa_{1g}$ parameter goes through zero in the region in question. This takes place in the inflection points of a field line (where its curvature becomes zero).

As can be seen from Figs. 2 and 4, there are four such points on a field line. Two are located near the current sheet, while the other two are at a distance from the current sheet. A higher-order correction should be taken into account near these points to regularize the singularity in the relation equation (10) between the φ and ψ potentials. This feature of the structure of the oscillation field components can be used to determine the inflection points of geomagnetic field lines from satellite observations of poloidal ULF oscillations and to find the location of the current sheet boundaries.

It should be noted that real SMS waves are strongly dissipative, which is impossible to take into account in the ideal MHD framework used in our calculations. In the real magnetosphere, therefore, the dominance of the small-scale component near the ionosphere will not be so obvious as in the structures calculated here. Variations in the oscillation structure will also be smooth enough in the current sheet, given the actual dissipation of SMS waves. These features will still manifest themselves to some degree, however, and can be used to identify these coupled modes in satellite-observed ULF oscillations.

Figure 5 shows the dependence of frequencies Ω_1, Ω_2 of the first two harmonics of standing waves of the coupled modes in hand on magnetic shell parameter $L = a/R_E$. Note the difficulty of computing the eigen solutions of (15). Each root $\Omega_N(L)$, corresponding to a large-scale Alfvén mode in the inner magnetosphere, is split into many "branches" in the transition region of the current sheet exhibiting a different structure of their small-scale components. As a result, the Newton gradient method we used to find the solutions with two eigenvalues is very sensitive to the initial parameters of the problem we employed. Therefore, we cannot track the behavior of each of the solutions continuously in the entire computational domain. However, an appropriate choice of the initial parameters can minimize the number of jumps from one branch to another. Regions of existence for all possible branches obtained by integrating the solutions for various large-scale modes may overlap.

The solutions in Fig. 5 corresponding to harmonics Ω_1 and Ω_2 are neutrally stable outside ($\mathrm{Im}(\Omega_{1,2}) = 0$), but become unstable inside the current sheet ($\mathrm{Im}(\Omega_{1,2}) > 0$). This phenomenon is a ballooning instability of Alfvén oscillations in the current sheet. As can be seen, the instability in question is not associated with any coupling between Alfvén and SMS oscillations, as was assumed previously (see Ohtani et al. 1989; Liu 1997). Coupled Alfvén and SMS modes become unstable only within the current sheet when the conditions of ballooning instability are satisfied for them. A similar problem was solved in Leonovich and Kozlov (2013b) in the WKB approximation. In that approximation there is no coupling of the oscillations in question. It was shown, however, that in the geotail model under study both the Alfvén and SMS waves can independently become unstable in the current sheet.

In the next section we show that coupling between modes occurring in the current sheet takes the form of their linear transformation and is described by a different formalism from the WKB approximation. Thanks to high dissipation of SMS waves, this coupling should have the opposite effect—it should result in Alfvén wave attenuation, competing with ballooning instability. Note that this instability cannot be regarded as an instability of the eigen oscillations of the plasma configuration under study. As will be shown in Sect. 5, the presence of this instability can increase the amplitude of the oscillations under study when moving from the poloidal resonance shell across magnetic shells.

For comparison, the same Fig. 5 shows the distributions of toroidal Alfvén wave frequencies Ω_{T1}, Ω_{T2}, the eigenvalues of the problem

$$\widehat{L}_T(\omega = \Omega_{TN})\varphi = 0$$

with ideal boundary conditions on the ionosphere. Comparing eigen-frequencies Ω_1, Ω_2 to Ω_{T1}, Ω_{T2} shows that the resonant shells for toroidal and poloidal standing Alfvén waves with the same frequency are very far spaced in the geotail model. Waves generated on the poloidal resonant shell are not capable of retaining an appreciable amplitude by the time they reach the toroidal resonant shell. They will be absorbed near the poloidal resonant shell due to ionospheric dissipation. When resolving the structure of these

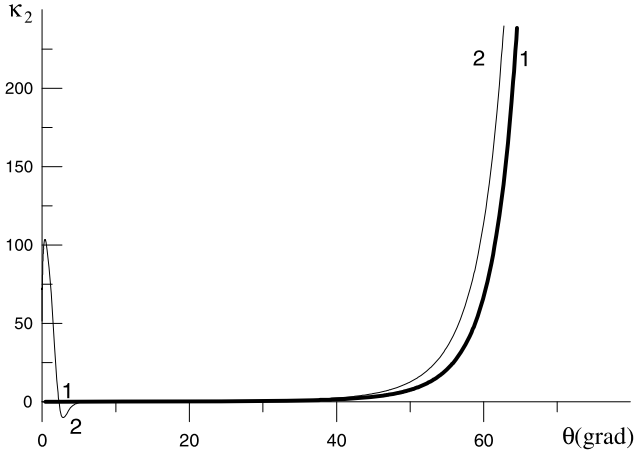

Fig. 6 The longitudinal distribution of the κ_2 coefficient for the fundamental harmonics of coupled modes ($N = 1$) on magnetic shells (1) $L = 6$ (*thick line*) and (2) $L = 15$ (*thin line*)

oscillations across magnetic shells, therefore, we can restrict ourselves to dealing with the structure in the neighborhood of the poloidal resonant shell.

4 The linear transformation of Alfvén and slow magnetosonic waves in the current sheet

Let us conduct a qualitative examination of some features of the spatial structure of oscillations under study in the current sheet. As is shown in the previous section, in most of the field line their structure is determined by the large-scale component corresponding to a poloidal Alfvén wave. Beyond the current sheet $C_S^2 \approx S^2 \ll A^2$ and $|\kappa_0 \bar{L}^4|$, $|\kappa_1 \bar{L}^3|$, $|\kappa_2 \bar{L}^2| \gg |\kappa_3 \bar{L}| \sim 1$, where $\bar{L}$ is the typical field line length. Therefore, in the qualitative study we can neglect the first two terms with higher derivatives in almost the entire field line, in Eq. (15):

$$\left[\kappa_2 \nabla_l^2 + \kappa_1 \nabla_l + \kappa_0\right] H \approx 0, \tag{18}$$

which, in the leading order, reduces to the well-known equation for poloidal Alfvén waves $\widehat{L}_P H \approx 0$. The solution of (18) in the WKB approximation has the form

$$H \approx \frac{1}{(\kappa_0/\kappa_2)^{1/4}} \exp\left[\pm i \int \sqrt{\kappa_0/\kappa_2}\, dl - \frac{1}{2}\int \frac{\kappa_1}{\kappa_2} dl\right]. \tag{19}$$

Let us examine the distribution of the κ_2 parameter along a field line. Figure 6 illustrates such distributions for the fundamental harmonics of coupled modes ($N = 1$) on two magnetic shells $L = 6$ and $L = 15$ discussed above. In the current sheet region, $S^2 \gg C_S^2 \approx A^2$, and the main feature of the κ_2 coefficient is that it goes through zero at some points $l = l_0$. It is evident that in the vicinity of l_0 the chosen approximation is not valid and higher derivatives must be taken account of in (15). Points l_0 are special points of Eq. (19) and singular turning points for the azimuthally small-scale Alfvén wave (see Leonovich and Mazur 1993).

For a qualitative study of the solution in the vicinity of points $l = l_0$, we keep the highest derivative in (15), which provides for regularizing the solution. Keeping the third derivative leads to a small correction in the position of these points. Linearizing the coefficients of such an equation in the vicinity of $l = l_0$, we write it as

$$\left[\nabla_z^4 + z\nabla_z^2 + \alpha_1 \nabla_z + \alpha_0\right] H_N \approx 0, \tag{20}$$

where these notations are introduced: $z = (l - l_0)/\lambda + i\lambda^2 \operatorname{Im}(\kappa_2(l_0))$, $\lambda = (\partial \operatorname{Re}(\kappa_2)/\partial l)_{l_0}^{-1/3}$, $\alpha_1 = \kappa_1(l_0)\lambda^3$, $\alpha_0 = \kappa_0(l_0)\lambda^4$. Equation (20) has a standard form for using the contour integral technique to search for its solution (Erokhin and Moiseev 1966; Leonovich and Mazur 1995). Let us seek the solution of (20) in the form

$$H_N\left(x^1, z\right) = \int_{\tilde{C}} \tilde{H}_N(s) e^{sz} ds, \tag{21}$$

where $\tilde{C}$ is an arbitrary path in the plane of complex s. Substituting (20) into (21) and using integration by parts in the second term, we have the following equation for $\tilde{H}_N$

$$s^2 \tilde{H}_N - \frac{\partial s^2 \tilde{H}_N}{\partial s} + \alpha_1 s \tilde{H}_N + \alpha_0 \tilde{H}_N = 0, \tag{22}$$

with the constraint

$$s^2 \tilde{H}_N e^{sz}\big|_{\tilde{C}} = 0, \tag{23}$$

that is the condition for choosing path $\tilde{C}$. Path $\tilde{C}$ must be such that either expression (23) vanish at its end or its start and end points coincide. The solution of (22) takes the form

$$\tilde{H}_N = \frac{1}{s^{2-\alpha_1}} \exp\left(\frac{s^3}{3} - \frac{\alpha_0}{s}\right), \tag{24}$$

and corresponding solution to (21) is

$$H_N\left(x^1, z\right) = \int_{\tilde{C}} \exp\left(\frac{s^3}{3} - \frac{\alpha_0}{s} + sz\right) \frac{ds}{s^{2-\alpha_1}}, \tag{25}$$

and the condition for selecting paths $\tilde{C}$

$$s^{\alpha_1} \exp\left(\frac{s^3}{3} - \frac{\alpha_0}{s} + sz\right)\Big|_{\tilde{C}} = 0.$$

Let us write complex variable s as $s = r_s e^{i\psi_s}$. It follows that expression (23) vanishes with $s \to 0$ in the region $-\pi/2 < \psi_s < \pi/2$ provided $\operatorname{Re}\alpha_0 > 0$ and in the sector $\pi/2 < \psi_s < 3\pi/2$ provided $\operatorname{Re}\alpha_0 < 0$. With $s \to \infty$, there are sectors $\pi/6 < \psi_s < \pi/2$, $5\pi/6 < \psi_s < 7\pi/6$, and $3\pi/2 < \psi_s < 11\pi/6$. They are white in Fig. 7. We will not construct the full set of solutions of (20), as was done in Erokhin and Moiseev (1966), Leonovich and Mazur (1995). We focus on those paths $\tilde{C}$ corresponding to path integrals (21) which describe the solutions with coupled modes.

Let us use the saddle-point method to estimate the value of path integrals (21) under $|z| \to \infty$ (see Budden 1985). Saddle points of (21) correspond to the zeros of the integrand exponent index

$$s^2 + \frac{\alpha_0}{s^2} + z = 0.$$

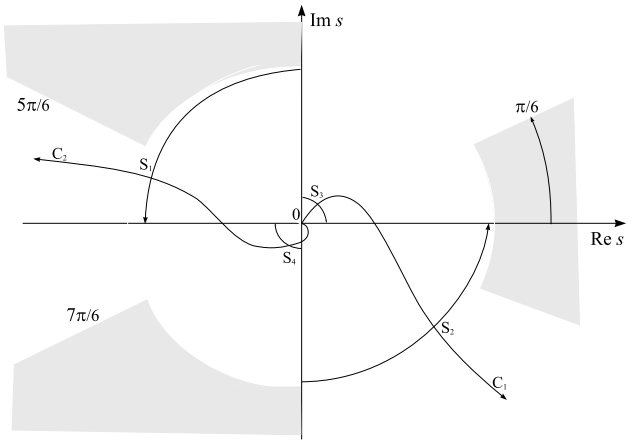

Fig. 7 Azimuth variations of saddle points S_i $(i = 1, 2, 3, 4)$ from (25) in the course of the transition from $\mathrm{Re}\, z \to \infty$ to $\mathrm{Re}\, z \to -\infty$ and the paths $\tilde{C}_{1,2}$ used in solving Eq. (21) when $\mathrm{Re}\, \alpha_0 > 0$

Consequently,

$$s^2 = -\frac{z}{2} \pm \sqrt{\frac{z^2}{4} - \alpha_0}.$$

When $\mathrm{Re}\, z \to \infty$, we have four saddle points $S_{1,2} = \pm i\sqrt{z}$ and $S_{3,4} = \pm i\sqrt{\alpha_0/z}$ (for $\mathrm{Re}\, \alpha_0 > 0$). The z value is complex in the general case, its imaginary part determined by complex frequency ω. The bypass rule for singular point $z = 0$ when passing from $\mathrm{Re}\, z \to \infty$ to $\mathrm{Re}\, z \to -\infty$ is defined in the same manner as when $\mathrm{Im}\, \omega > 0$, i.e. the phase of z varies 0 to π. Thus, when $\mathrm{Re}\, z \to -\infty$, the saddle points transform into $S_{1,2} = \mp\sqrt{-z}$, $S_{3,4} = \pm\sqrt{-\alpha_0/z}$, as shown in Fig. 7.

Let us choose path $\tilde{C}_1$ and $\tilde{C}_2$ as shown in Fig. 7. Both paths cross two saddle points and describe coupled Alfvén and SMS modes. Let us denote $\alpha_0 = r_\alpha e^{i\nu}$. Using the saddle-point method procedure for estimating the integrals, and given the contribution of both points, produces the following asymptotics for the solution of (20):

$$H_N^{(1)} = \begin{cases} \frac{z^{1/4-\alpha_1/2}}{\alpha_0^{3/4-\alpha_1/2}} \exp[2i\sqrt{\alpha_0 z} + i\varphi_{A1}] \\ \quad + \frac{\exp[-\frac{2}{3}iz^{3/2}+i\varphi_{S1}]}{z^{5/4-\alpha_1/2}}, \quad \mathrm{Re}\, z \to \infty, \\ \frac{(-z)^{1/4-\alpha_1/2}}{\alpha_0^{3/4-\alpha_1/2}} \exp[-2\sqrt{-\alpha_0 z} + i\varphi_{A2}] \\ \quad + \frac{\exp[-\frac{2}{3}(-z)^{3/2}+i\varphi_{S2}]}{(-z)^{5/4-\alpha_1/2}}, \quad \mathrm{Re}\, z \to -\infty, \end{cases}$$

$$H_N^{(2)} = \begin{cases} \frac{z^{1/4-\alpha_1/2}}{\alpha_0^{3/4-\alpha_1/2}} \exp[-2i\sqrt{\alpha_0 z} + i\varphi_{A3}] \\ \quad + \frac{\exp[\frac{2}{3}iz^{3/2}+i\varphi_{S3}]}{z^{5/4-\alpha_1/2}}, \quad \mathrm{Re}\, z \to \infty, \\ \frac{(-z)^{1/4-\alpha_1/2}}{\alpha_0^{3/4-\alpha_1/2}} \exp[2\sqrt{-\alpha_0 z} + i\varphi_{A4}] \\ \quad + \frac{\exp[\frac{2}{3}(-z)^{3/2}+i\varphi_{S4}]}{(-z)^{5/4-\alpha_1/2}}, \quad \mathrm{Re}\, z \to -\infty, \end{cases} \tag{26}$$

where the notations are: $\varphi_{A1} = (\pi + \nu)/4$; $\varphi_{A2} = \nu/4 - \alpha_1\pi/2$; $\varphi_{A3} = \nu/4 + \alpha_1\pi + 3\pi/4$; $\varphi_{A4} = \nu/4 + \alpha_1\pi/2 + \pi/2$; $\varphi_{S1} = \alpha_1\pi + 3\pi/4$; $\varphi_{S2} = 3\alpha_1\pi/2$; $\varphi_{S3} = \pi/4$; $\varphi_{S4} = (\alpha_1 - 1)\pi/2$. The upper lines in (26) describe the field of Alfvén and SMS waves in the transparency region $(\mathrm{Re}\, z \to \infty)$, and the lower lines refer to the opacity region $(\mathrm{Re}\, z \to -\infty)$. Linearizing coefficients $\kappa_{0,1,2}$ in the vicinity of $l = l_0$ in (19), the WKB solution under $\mathrm{Re}\, z \to 0$ can be represented in the form

$$H_N \sim z^{1/4-\alpha_1/2} \exp(\pm 2i\sqrt{\alpha_0 z}).$$

The inner asymptotics of the WKB solutions (19) is matched with the outer asymptotics of the first terms in (26). Hence, the first terms in (26) correspond to the field of Alfvén waves and the second terms, to the SMS field.

In the vicinity of points $l = l_0$, a partial linear transformation takes place of Alfvén waves into SMS waves. There can be a number of such points in the current sheet. Notably, this transformation differs from the resonant interaction of modes such as the Alfvén and magnetosonic resonances. Since $C_s \approx A$ in the current sheet, the typical spatial structures of Alfvén and SMS waves become similar, with no dramatic increase in the oscillation amplitudes.

The linear transformation can take place even if there are no transformation points. As depicted in Fig. 6, coefficient κ_2 does not go through zero anywhere on magnetic shell $L = 6$. However, a small-scale component is still present in the solutions in Figs. 3 and 4. This is due to the fact that the linear transformation occurs when the κ_2 coefficient becomes sufficiently small somewhere on the field line. Figure 6 shows that this occurs in the equatorial region on magnetic shell $L = 6$. Therefore, the entire current sheet region is the region of a linear transformation of Alfvén and SMS waves.

It is impossible to use such a formalism for precise calculations of wave fields, since the asymptotics are beyond the computational domain. However, this formalism provides an opportunity to understand the inner mechanism of coupling of the guided modes.

5 The structure of coupled MHD modes across magnetic shells

Let us determine the spatial structure of the oscillations under study across magnetic shells. In order to do that, we need to find the solution of the full Eq. (8) with boundary conditions both on the ionosphere and on the asymptotics over the transverse x^1 coordinate. Let us define the boundary conditions. If a solution to (12) is found on some magnetic shell $x^1 = \bar{x}^1$, with the above-defined boundary conditions, the natural requirement would be for the amplitude of the monochromatic wave field to be limited away from this

shell. For complex-frequency eigen oscillations (with no external source) it is demonstrably impossible to construct a solution to (8) that would satisfy the boundary conditions for both asymptotics $(x^1 - \bar{x}^1) \to \pm\infty$. A solution limited on one of the asymptotics is sure to increase on the other.

If there is a broadband source for $m \gg 1$ Alfvén waves, however, its spectrum including the frequency $\omega = \mathrm{Re}(\Omega_N)$, then this source will generate a poloidal standing Alfvén wave on the magnetic shell $x^1 = x^1_N$ (Leonovich and Mazur 1993). In the current sheet, the Alfvén wave partially transforms into the SMS wave. As a result, a coupled mode forms along the field line. The magnetic shell $x^1 = x^1_N$ is a turning shell that separates the transparency and opacity regions for such waves over the x^1 coordinate. The transparency region is located between the poloidal $(x^1 = x^1_N)$ and toroidal $(x^1 = x^1_{TN})$ resonant surfaces of the N-th harmonic of standing Alfvén waves (see Fig. 5). The distance between these surfaces on magnetic shells in the region of the current sheet is rather large. Hence we can restrict ourselves to exploring the structure in the vicinity of the poloidal resonant shell.

The wave generated on the poloidal resonant shell runs through the transparency region to the toroidal resonant shell. The shell $x^1 = x^1_{TN}$ is a singular turning shell, the wave is completely absorbed in its vicinity. Such a wave has the structure of a traveling wave across magnetic shells in the transparency region, but remains a standing wave along magnetic field lines.

Let us construct a solution describing the structure of (generally unstable) azimuthally small-scale coupled Alfvén and SMS waves in the vicinity of the poloidal resonant shell. In the leading order of the perturbation theory, we sought the structure of the oscillations in hand along magnetic field lines with the ideal boundary conditions on the ionosphere. Their structure across magnetic shells can be found in the next, first, order. In the boundary conditions we take into account the finite conductivity of the ionosphere and the presence of external currents (see (11)).

Let us seek the solution of (8) for the N-th harmonic of standing coupled modes in the form

$$\varphi_N = U_N\big(x^1\big)\big[H_N\big(x^1, x^3\big) + h_N\big(x^1, x^3\big)\big], \tag{27}$$

where the function $H_N(x^1, x^3)$ describes the structure of the standing wave in the zeroth approximation, and the function $h_N(x^1, x^3)$ is the first-order correction accounting for the non-ideality of the boundary conditions on the ionosphere

$$h_N\big(x^1, l_\pm\big) = \mp i\frac{v_\pm}{\omega}\frac{\partial H_N}{\partial l}\bigg|_{l_\pm} - \frac{J^\pm_\parallel}{V_\pm}U_N^{-1}\big(x^1\big). \tag{28}$$

In the leading order of the perturbation theory we solved the equation:

$$\widehat{L}_S(\Omega_N)\widehat{L}_P(\Omega_N)H_N + \widehat{L}_C(\Omega_N)H_N = 0.$$

Substituting the solution in the form (27) into (8) yields, in the first order of the perturbation theory

$$\begin{aligned}&\nabla_1^2 U_N\big(x^1\big)\widehat{L}_T(\Omega_N)H_N\\ &\quad - k_2^2 U_N\big(x^1\big)p^{-1}\frac{(\omega^2 - \Omega_N^2)}{A^2}H_N\\ &\quad - k_2^2 U_N\big(x^1\big)\widehat{L}_P(\Omega_N)h_N \approx 0.\end{aligned}$$

We take into account that in most of the field line $C_S \ll A$ and $|\widehat{L}_S(H_N + h_N)| \approx |\Omega_N^2(H_N + h_N)/C_S^2| \gg |\widehat{L}_C(\Omega_N) \times (H_N + h_N)|$. Multiplying this equation by H_N and integrating along the field line between the magnetoconjugated ionospheres, we get

$$\beta_N\nabla_1^2 U_{Pn} + k_2^2\big[\alpha_N\big(\omega^2 - \Omega_N^2\big) + \bar{\delta}_N\big]U_N = 0, \tag{29}$$

where these notations are introduced

$$\alpha_N = \int_{l_-}^{l_+}\frac{H_N^2}{pA^2}dl,$$

$$\beta_N = -\int_{l_-}^{l_+}H_N\widehat{L}_T(\Omega_N)H_N dl,$$

$$\bar{\delta}_N = \int_{l_-}^{l_+}H_N\widehat{L}_P(\Omega_N)h_N dl = -\frac{h_N}{p}\frac{\partial H_N}{\partial l}\bigg|_{l_-}^{l_+}.$$

Taking into account the boundary conditions (28) and choosing the normalization of eigenfunctions H_N such that $\alpha_N = 1$, we get the equation

$$\nabla_1^2 U_N + \frac{k_y^2}{\omega^2}\big[(\omega + i\gamma_N)^2 - \Omega_N^2\big]U_N = I_{\parallel N}, \tag{30}$$

which describes the structure of standing azimuthally small-scale waves over the x^1 coordinate in the vicinity of the poloidal resonant shell. Here $k_y^2 = k_2^2\omega^2/\beta_N$,

$$\gamma_N = \frac{1}{2\omega^2}\left[\frac{v_+}{p_+}\left(\frac{\partial H_N}{\partial l}\right)_+^2 + \frac{v_-}{p_-}\left(\frac{\partial H_N}{\partial l}\right)_-^2\right]$$

is the decrement of Alfvén waves due to the finite ionospheric conductivity in the vicinity of the poloidal shell,

$$I_{\parallel N} = \frac{k_y^2}{\omega^2}\left[\frac{J^+_\parallel}{p_+V_+}\left(\frac{\partial H_N}{\partial l}\right)_+ - \frac{J^-_\parallel}{p_-V_-}\left(\frac{\partial H_N}{\partial l}\right)_-\right]$$

is the function describing the source of Alfvén waves related to external currents in the ionosphere.

Let us write $\Omega_N = \bar{\Omega}_N + i\delta_N$, where $\bar{\Omega}_N \equiv \mathrm{Re}(\Omega_N)$, $\delta_N \equiv \mathrm{Im}(\Omega_N)$. In the vicinity of the resonant shell $x^1 = x^1_N$, we then use the following approximate linear decomposition:

$$\bar{\Omega}_N^2 \approx \omega^2\left(1 - \frac{x^1 - x^1_N}{a_N}\right),$$

where $a_N = (\nabla_1 \ln\bar{\Omega}_N^2)^{-1}$ is the typical variation scale of $\bar{\Omega}_N$ at $x^1 = x^1_N$. Substituting this decomposition into Eq. (30) and introducing the dimensionless transverse coordinate $\xi = (x^1 - x^1_N)/\Delta_N$ (where $\Delta_N = a_N^{1/3}/k_y^{2/3}$), it is possible to represent it in the form

$$\frac{\partial^2}{\partial\xi^2}U_N + (\xi + i\varepsilon_N)U_N = \frac{a_N^{2/3}}{k_y^{4/3}}I_{\parallel N}, \tag{31}$$

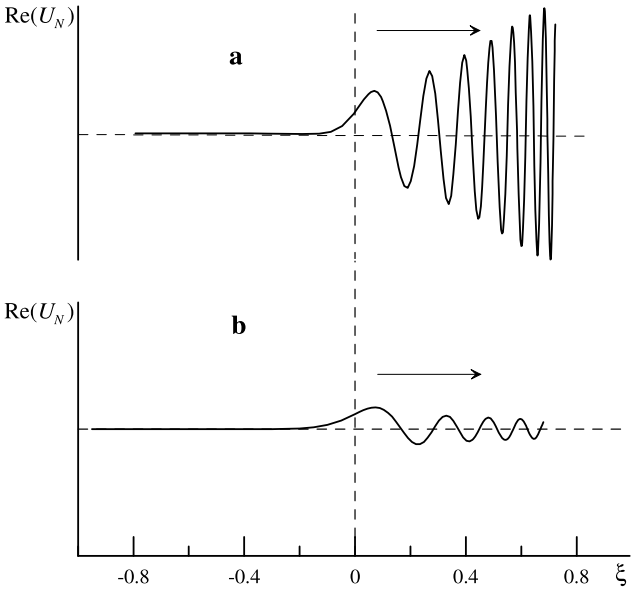

Fig. 8 The structure of coupled poloidal guided modes across magnetic shells: (**a**) the wave has a larger instability increment than its decrement due to ionospheric dissipation ($\varepsilon_N > 0$); (**b**) the wave has a smaller instability increment than its decrement due to ionospheric dissipation ($\varepsilon_N < 0$)

where $\varepsilon_N = 2(\gamma_N - \delta_N)(k_y a_N)^{2/3}/\omega$. The localization of the wave source in the ionosphere is assumed to be much larger than their transverse wave length. On the scale of the localization of the solution, the right-hand part of (31) can then be assumed to be constant. The solution of (31) satisfying the given boundary conditions (the limited amplitude on the asymptotics) is

$$U_N\left(x^1\right) = \frac{a_N^{2/3}}{k_y^{4/3}} I_{\|N} G(\xi + i\varepsilon_N), \tag{32}$$

where $G(\zeta)$ is the solution of the nonuniform Airy equation which has the following integral representation:

$$G(\zeta) = -i\int_0^\infty \exp\left[-i\frac{s^3}{3} + is\zeta\right] ds. \tag{33}$$

Its asymptotics are

$$G(\zeta) = \begin{cases} -\frac{\pi^{1/2}}{\zeta^{1/4}} \exp(\frac{2}{3} i\zeta^{3/2} + i\frac{\pi}{4}), & \operatorname{Re}\zeta \to \infty, \\ \zeta^{-1}, & \operatorname{Re}\zeta \to -\infty. \end{cases}$$

It follows immediately that the solution (32) decreases as a power law in the opacity region, and describes a wave running from the resonant shell in the transparency region. The structure of the solution across magnetic shells is presented in Fig. 8. If the growth rate of the ballooning instability of coupled modes in question is larger than their decrement due to ionospheric dissipation ($\varepsilon_N > 0$), the amplitude would increase away from the resonant shell (Fig. 8a). That is the case only on magnetic shells where the condition of the existence of unstable modes is valid ($|k_2| > |k_1|$). The farther from the resonance shell, the larger is k_1 and somewhere on the way the wave structure suffers a transition to a state with $|k_2| < |k_1|$. After that, the wave amplitude starts to decrease towards the toroidal resonant shell. If $\varepsilon_N < 0$, the wave amplitude starts to decrease directly after leaving the poloidal resonant shell (Fig. 8b).

6 Conclusion

Let us now summarize the main results of the paper.

1. The problem is solved of the structure of coupled Alfvén and slow magnetosonic modes on tailward-stretched field lines.
2. It is shown that the mode coupling occurs in the region of the current sheet in the magnetotail and that these modes are not coupled on most of the field line.
3. Due to the high conductivity of the ionosphere, the field of the coupled modes forms standing waves along magnetic field lines. On most of the field line, a large-scale Alfvén wave structure dominates. A small-scale SMS wave structure manifests itself near the ionosphere and in the current sheet. This feature can be used to identify such coupled modes in ULF oscillations observed by satellites. This finding is rather unexpected because some previous papers suggested that a small-scale structure is only dominant in the current sheet.
4. At the field lines crossing the current sheet the structure of the field components of poloidal coupled modes has singularities at the inflection points of a field line. They look like resonance peaks. There are four such points on a field line. Two of them are in the vicinity of the current sheet. It is possible to use them for determining the approximate position of the boundaries of the current sheet in satellite observations of ULF oscillations.
5. In the transition region between the inner magnetosphere and the current sheet, the spectrum of lower harmonics of standing waves splits into numerous branches differing in the structure of their small-scale components. These oscillations become unstable in the current sheet region, which is a manifestation of the ballooning instability.
6. The coupled modes under scrutiny can be driven in the magnetosphere in the presence of an external source. In this paper, external currents in the Earth's ionosphere are used as such a source. Across magnetic shells, the structure of such oscillations is a running wave from the resonance shell. When the ballooning instability-induced growth rate is larger than their decrement due to dissipation in the ionosphere, the amplitude of the oscillations increases away from the resonant shell. In the opposite case, the oscillation amplitude decreases.
7. The presence of a ballooning instability could be considered as a possible mechanism of magnetic reconnection

in the current sheet. However, the very presence of this instability needs further investigation, because the dissipation of SMS waves due to their interaction with the background ions was not taken into account in the problem solved in this paper.

Acknowledgements This work was partially supported by RFBR grant #12-02-00031- and by Program #22 of the presidium of the Russian Academy.

Appendix A: The axisymmetric model of the geotail with a current sheet

Let us define the magnetic field model as follows. In the meridional plane, a magnetic field line is described by radius $r(a,\theta)$ from the Earth's center (Fig. 1), where a is the equatorial radius of a field line, θ is its latitude as counted from the equator. We consider a model magnetosphere that is symmetric about the equatorial plane. The shape of the dipole magnetic field line is described by $r \equiv r_d = a\cos^2\theta$, while its strength is

$$B_d = \bar{B}_d\left(\frac{R_E}{a}\right)^3 \frac{\sqrt{1+3\sin^2\theta}}{\cos^6\theta},$$

where $\bar{B}_d = 0.32$ G is the magnetic field strength at the Earth's equator (R_E is the Earth's radius). The subsequent calculations will also invoke the cylindrical coordinate system (ρ,ϕ,z) (see Fig. 1). The dipole magnetic field components in this coordinate system $\mathbf{B}_d = (B_{d\rho}, 0, B_{dz})$ are

$$B_{d\rho} = B_d * \cos\tilde{\theta}, \qquad B_{dz} = B_d * \sin\tilde{\theta},$$

where $\tilde{\theta} = \arccos(3\sin\theta\cos\theta/\sqrt{1+3\sin^2\theta})$ is the angle between the tangent to the field line and the ρ axis.

In order to model the magnetic field $\mathbf{B}_j = (B_{j\rho}, 0, B_{jz})$ induced by an azimuthal current, we use the following model for the magnetic field $B_{j\rho}$ component

$$B_{j\rho} = \frac{B_{j\infty}}{2}\left[1+\tanh\frac{\rho-\tilde{\rho}}{\Delta_\rho}\right]\tanh\frac{z}{\Delta},$$

where $\tilde{\rho} \approx 10\ R_E$ is the near-Earth boundary of the plasma sheet, $\Delta_\rho \approx 2R_E$ is the typical thickness of the transition region, Δ is the typical thickness of the current sheet (see Fig. 1), $B_{j\infty} \approx 20$ nT is the magnetic field in the magnetotail lobes away from the current sheet. The current sheet thickness is known to vary over a wide range (Birn 2011), $\Delta \sim 1$–$2\ R_E$ for quiet geomagnetic conditions (thick current sheet) to $\Delta \sim 0.1$–$0.4\ R_E$ in a disturbed magnetosphere (thin current sheet). In the numerical calculations here, we restrict ourselves to the model with a thin current sheet where $\Delta = 0.2\ R_E$, for which mode coupling and ballooning instability were most conspicuous.

Since the magnetic field of a current obeys this equation

$$\operatorname{div}\mathbf{B}_j = \frac{1}{\rho}\frac{\partial\rho B_{j\rho}}{\partial\rho} + \frac{\partial B_{jz}}{\partial z} = 0,$$

we have

$$B_{jz} = -\frac{B_{j\infty}\Delta}{2}\left[\frac{1}{\rho}\left(1+\tanh\frac{\rho-\tilde{\rho}}{\Delta_\rho}\right) + \frac{1}{\Delta_\rho\cosh^2(\rho-\tilde{\rho})/\Delta_\rho}\right]\ln\cosh\frac{z}{\Delta}.$$

The B_{jz} component has a singularity at $\rho \to 0$ and $z \to \infty$. In the region of stretched field lines ($\Delta \ll \rho$, $z < \rho$), however, the contribution of this component is negligible. Of course, in the real magnetosphere, magnetic field has no singularity, its distribution is determined not only by the sheet current but also by currents at the magnetospheric boundary. It is possible to obtain a similar distribution for the background magnetic field by introducing equivalent shell currents away from the current sheet. Calculation of the spatial distribution of such currents is, however, a rather complicated problem, which is beyond the scope of the problem formulated here.

The leading term of the axisymmetric azimuthal current $\mathbf{j} = (0, j_\phi, 0)$ corresponding to the above-described magnetic components is

$$j_\phi = \frac{c}{4\pi}(\operatorname{curl}\mathbf{B}_0)_\phi \approx \frac{cB_{j\infty}}{8\pi}\frac{1}{\Delta\cosh^2(z/\Delta)}\left[1+\tanh\frac{\rho-\tilde{\rho}}{\Delta_\rho}\right].$$

This term describes the azimuthal current localized near the equatorial plane at scale Δ.

Hence, the total background magnetic field $\mathbf{B}_0 = (B_{0\rho}, 0, B_{0z})$ has the following components: $B_{0\rho} = B_{d\rho} + B_{j\rho}$, $B_{0z} = B_{dz} + B_{jz}$. The shape of the field line is defined by (see for details Leonovich and Kozlov 2013b):

$$r(a,\theta) = a\exp\left[\int_0^\theta \frac{\sin\theta'\cos\theta' - \sin\bar{\theta}\cos\bar{\theta}}{\sin^2\bar{\theta} - \sin^2\theta'}d\theta'\right], \tag{34}$$

where $\bar{\theta}$ is the angle between the tangent to the field line and the ρ axis ($\sin\bar{\theta} = B_{0z}/B_0$, $\cos\bar{\theta} = B_{0\rho}/B_0$).

Expressions for the metric tensor components in the (a,ϕ,θ) system tied to the magnetic field geometry have the form

$$g_1 = \frac{r^2(a,\theta)}{r^2(a,\theta) + (\partial r/\partial\theta)^2}\left(\frac{\partial r}{\partial a}\right)^2, \tag{35}$$

$$g_2 = r^2(a,\theta)\cos^2\theta. \tag{36}$$

Deriving the g_3 component is more complicated. Note that the expression for $g_3(a,\theta)$ derived in Leonovich and Kozlov (2013b) only applies to fields with scalable field lines, such as dipole-like magnetic fields. In our calculations we only used the logarithmic derivative

$$\bar{\varkappa}_{1g} = \frac{\varkappa_{1g}}{\sqrt{g_1}} = \frac{\nabla_1(\ln g_3)}{\sqrt{g_1}} = 2/r_c, \tag{37}$$

where

$$r_c = \frac{[r^2 + (r')^2]^{3/2}}{r^2 + 2r'^2 - rr''},$$

is the curvature radius of the field line, $r' \equiv \partial r/\partial\theta$. Note that the (a, ϕ, θ) coordinates are non-orthogonal, but are unambiguously linked to the (x^1, x^2, x^3) coordinates. In particular, the derivatives of the medium parameters with respect to the x^1 coordinate in the (a, θ) system have the form

$$\nabla_1 f = \left(\frac{\partial f}{\partial a}\right)_\theta - \left(\frac{\partial f}{\partial \theta}\right)_a \frac{(\partial r/\partial\theta)_a (\partial r/\partial a)_\theta}{r^2(a,\theta) + (\partial r/\partial\theta')_a^2},$$

where the subscripts indicate that the corresponding derivative is taken at constant a and θ.

Let us simulate the Alfvén speed distribution as follows. In the region where the dipole component dominates in the magnetic field (that is $\rho < \tilde{\rho}$) let $A(a, \theta) \equiv A_d = A_i/r_d(a, \theta)$, where $A_i \approx 5000$ km/s is the Alfvén speed at the upper ionospheric boundary ($r_i = R_E + 1500$ km), r_d is the radius of the dipole field line. This simple model simulates rather accurately the distribution of A along the field line from the ionosphere to the equatorial plane. Of course, it does not take into account the drastic change in A at the plasmapause, but we will not consider this region of the magnetosphere.

In the current sheet region ($\rho > \tilde{\rho}$), Alfvén speed A depends primarily on the z coordinate. The value of A changes from $A_0 \approx 100$ km/s in the current sheet ($z = 0$) to $A_\infty \approx 6000$ km/s in the magnetotail lobes (for $z \gg \Delta$, where Δ is the typical current sheet thickness). Let us model the Alfvén speed as follows, in this region:

$$A(z) \equiv A_t = A_0\big[1 - \big(1 - (A_\infty/A_0)\big)\tanh(z/\Delta)\big].$$

The complete model of the Alfvén speed can be presented as

$$A(\rho, z) = \frac{1}{2}\left[A_d + A_t - (A_d - A_t)\tanh\frac{\rho - \tilde{\rho}}{\Delta_\rho}\right]. \qquad (38)$$

Equation (38) with a preassigned distribution of the magnetic field defines the plasma density distribution ρ_0.

To model the sound speed distribution requires specifying a model for the plasma pressure distribution. We define the plasma pressure distribution in a similar manner to what was done above for the Alfvén speed distribution, separately for the $\rho < \tilde{\rho}$ region, dominated by a dipole magnetic field, and for the $\rho > \tilde{\rho}$ region, dominated by the $B_{j\rho}(z)$ component. We neglect the magnetic field of the azimuthal current in the former region as we do the dipole magnetic field in the latter. Of course, this distribution of the equilibrium plasma pressure can only be regarded as approximate. As follows from (5), the pressure P_0 is conserved along magnetic field lines. If we could specify the exact distribution of pressure on some shell intersecting all of the field lines (for example, near the ionosphere), it would be defined in the whole model magnetosphere. Unfortunately, it does not seem possible to define such a distribution with good accuracy without taking into account the currents on the magnetospheric boundary. Therefore, in this paper we will employ the above method of approximately describing the equilibrium plasma pressure distribution.

Given the above assumptions and the fact that the dipole magnetic field is force-free, we have $P_0 \equiv P_{0d} = const$ in the $\rho < \tilde{\rho}$ region. As for the $\rho > \tilde{\rho}$ region, the equilibrium condition (5) yields

$$P_0(z) \equiv P_{0j}(z) = P_{0j}(\infty) - \frac{B_{j\rho}^2(z)}{8\pi} + \frac{B_{j\rho}^2(\infty)}{8\pi},$$

where $P_{0j}(\infty)$ is the plasma pressure in the magnetotail lobes away from the current sheet. Let us select $P_{0j}(\infty)$ such that $\beta_\infty = 8\pi P_{0j}(\infty)/B_{j\rho}^2(\infty) = 0.005$. The above-derived distribution of $P_0(z)$ corresponds to the Harris layer model, believed to be a good enough approximation for describing the geotail current sheet. Since all MHD-oscillation instability effects are determined by the pressure distribution within, and next to, the current sheet, these results will, hopefully, not be very different from a more accurate model distribution of $P_0(\rho, z)$. Let us also set $P_{0d} = B_{j\rho}^2(\infty)/8\pi$, for definiteness. We will simulate the complete distribution $P_0(z)$ of plasma pressure using the formula

$$P_0(\rho, z) = \frac{1}{2}\left[P_{0d} + P_{0j} - (P_{0d} - P_{0j})\tanh\frac{\rho - \tilde{\rho}}{\Delta_\rho}\right]. \qquad (39)$$

Since the distribution of ρ_0 is defined by the Alfvén speed distribution, we can now construct the distribution of the sound speed in plasma.

Let us now examine the relations of the ionospheric field-aligned currents $j_\parallel$ to wave processes in the conducting ionospheric layer. Internal gravity and acoustic-gravity waves in the neutral atmosphere can act as such wave processes, their range of periods overlapping the range of the magnetospheric MHD oscillations in question. The ionosphere is partially ionized at the conductive layer level so that the collisions of plasma ions and electrons with neutral atoms play the main role in their dynamics. The electrons are magnetized ("tied" to magnetic field lines), and ions are non-magnetized in the process. The ion component moving across the magnetic field lines is determined by it being drawn by the neutral component, while the electrons remain immobile, in this direction. A transverse current results:

$$\mathbf{j}_\perp = en(\mathbf{v}_{i\perp} - \mathbf{v}_{e\perp}),$$

where $\mathbf{v}_{e\perp} \approx 0$ is the speed of electrons, $\mathbf{v}_{i\perp} \approx \mathbf{v}_{0\perp}$ is the speed of ions, $\mathbf{v}_{0\perp}$ is the speed of neutral gas in the wave process. The transverse conductivity of the ionospheric plasma, $\hat{\sigma}_\perp$, is tensorial in form. Therefore the relation of the transverse currents caused by atmospheric wave motions to transverse electric fields has the form

$$\mathbf{j}_\perp = \hat{\sigma}_\perp \mathbf{E}_\perp,$$

where

$$\hat{\sigma}_\perp = \begin{pmatrix} \sigma_{11} & \sigma_{12} \\ \sigma_{21} & \sigma_{22} \end{pmatrix},$$

σ_{ij} are the components of the Hall and Pedersen conductivity of the ionosphere for the wave process in question.

Since the longitudinal conductivity is much larger than transverse conductivity ($\sigma_\parallel \gg \sigma_\perp$) in a strongly inhomogeneous ionospheric plasma, the transverse currents are closed through magnetospheric field-aligned currents $j_\parallel$, that are in fact the generated Alfvén wave. Their value at the upper boundary of the ionosphere can be determined from the condition that the total current be closed

$$\operatorname{div} \mathbf{j} = 0,$$

which should be integrated over the thickness of the conductive ionospheric layer. Thus, knowing all the components of the total current and the expressions for the components of the conductivity tensor of a partially ionized plasma (see e.g. Alperovich and Fedorov 2007), we can determine the components of the oscillation electric field at the ionospheric altitude.

Appendix B: The coefficients of Eq. (15)

We write the coefficients of (15) in the following form

$$\kappa_3 = 3\varkappa_{lp} + \varkappa_{lb}, \tag{40}$$

$$\kappa_2 = \frac{\varkappa_{1g}\varkappa_{1B}}{g_1} + \varkappa_a^{(2)} + \varkappa_{ls}\varkappa_{la} + 2\varkappa_{lb}\varkappa_{lp} + 3p\nabla_l^2 p^{-1} + \omega^2\left(A^{-2} + C_s^{-2}\right), \tag{41}$$

$$\kappa_1 = \frac{\varkappa_{1g}\varkappa_{1B}}{g_1}\varkappa_{lc} + \varkappa_{lp}\varkappa_{ls}\varkappa_{la} + \varkappa_{lp}\varkappa_a^{(2)} + \varkappa_{lb}p\nabla_l^2 p^{-1} + p\nabla_l^3 p^{-1} + \omega^2\left(\frac{\varkappa_{lb}}{A^2} + \frac{\varkappa_{lp}}{C_s^2} + 2p\nabla_l\frac{p^{-1}}{A^2}\right), \tag{42}$$

$$\kappa_0 = \frac{\omega^4}{A^2C_s^2} + \omega^2\left(\frac{\varkappa_a^{(2)} + \varkappa_{ls}\varkappa_{la} - \varkappa_{1g}\varkappa_{1P}/g_1}{A^2} + \varkappa_{lb}p\nabla_l\frac{p^{-1}}{A^2} + p\nabla_l^2\frac{p^{-1}}{A^2}\right), \tag{43}$$

where the notations are

$$p = \sqrt{g_2/g_1},$$

$$\varkappa_{lp} = \nabla_l\left(\ln p^{-1}\right),$$

$$\varkappa_{la} = \nabla_l\left(\ln\frac{B_0}{\varkappa_{1g}}\right),$$

$$\varkappa_{ls} = \nabla_l\left(\ln\frac{\sqrt{g_1g_2}P_0^\sigma}{\rho_0}\right),$$

$$\varkappa_{lb} = \varkappa_{ls} + 2\varkappa_{la},$$

$$\varkappa_{lc} = \nabla_l\left(\ln\frac{\varkappa_{1B}B_0P_0^\sigma}{\rho_0}\right),$$

$$\varkappa_a^{(2)} = \frac{\varkappa_{1g}}{B_0}\nabla_l^2\frac{B_0}{\varkappa_{1g}},$$

and $\varkappa_{1g}$, $\varkappa_{1B}$ and $\varkappa_{1P}$ are determined by the expressions (9).

References

Agapitov, O., Glassmeier, K.-H., Plaschke, F., Auster, H.-U., Constantinescu, D., Angelopoulos, V., Magnes, W., Nakamura, R., Carlson, C.W., Frey, S., McFadden, J.P.: J. Geophys. Res. **114**, A00C27 (2009). doi:10.1029/2008JA013553

Alperovich, L.S., Fedorov, E.N.: Hydromagnetic Waves in the Magnetosphere and the Ionosphere vol. 353. Springer, New York (2007)

Birn, J.: In: The Dynamic Magnetosphere IAGA special Sopron Book Series, vol. 3, p. 49. Springer, New York (2011). doi:10.1007/978.94.007.0501.2.4

Blanc, M., Kallenbach, R., Erkaev, N.V.: Space Sci. Rev. **116**, 227 (2005). doi:10.1007/s11214-005-1958-y

Budden, K.G.: The Propagation of Radio Waves: The Theory of Radio Waves of Low Power in the Ionosphere and Magnetosphere, Cambridge University Press, Cambridge (1985)

Chen, L., Hasegawa, A.: J. Geophys. Res. **79**, 1024 (1974). doi:10.1029/JA079i007p01024

Cheremnykh, O.K., Parnowski, A.S.: Adv. Space Res. **37**, 599 (2006). doi:10.1016/j.asr.2005.01.073

Dmitrienko, I.S.: J. Plasma Phys. **79**, 7 (2013). doi:10.1017/S0022377812000608

Erkaev, N.V., Shaidurov, V.A., Semenov, V.S., Langmayr, D., Biernat, H.K.: Phys. Plasmas **12**(1), 012905 (2005). doi:10.1063/1.1833392

Erokhin, N.S., Moiseev, S.S.: J. Appl. Mech. Tech. Phys. **7**, 17 (1966). doi:10.1007/BF00916966

Guglielmi, A., Kangas, J., Kultima, J., Potapov, A.: J. Geophys. Res. **105**, 25185 (2000). doi:10.1029/2000JA900089

Hameiri, E., Laurence, P., Mond, M.: J. Geophys. Res. **96**, 1513 (1991). doi:10.1029/90JA02100

Kangas, J., Kultima, J., Guglielmi, A., Potapov, A., Hayashi, K.: Earth Planets Space **53**, 1177 (2001)

Kivelson, M.G.: In: Kamide, Y., Chian, A.C.-L. (eds.) Planetary Magnetospheres, p. 469. Springer, Netherlands, (2007)

Klimushkin, D.Y., Mager, P.N., Marilovtseva, O.S.: J. Atmos. Sol.-Terr. Phys. **72**, 1327 (2010). doi:10.1016/j.jastp.2010.09.019

Klimushkin, D.Y., Mager, P.N., Pilipenko, V.A.: Earth Planets Space **64**, 777 (2012). doi:10.5047/eps.2012.04.002

Korn, G.A., Korn, T.M.: Mathematical Handbook for Scientists and Engineers. Definitions, Theorems, and Formulas for Reference and Review. McGraw-Hill, New York (1968), 2nd enl. and rev. edition

Kozlov, D.A., Leonovich, A.S., Cao, J.B.: Ann. Geophys. **24**, 263 (2006). doi:10.5194/angeo-24-263-2006

Lee, D.-H., Lysak, R.L.: J. Geophys. Res. **104**, 28691 (1999). doi:10.1029/1999JA900377

Leonovich, A.S.: J. Geophys. Res. **106**, 25803 (2001). doi:10.1029/2001JA000104

Leonovich, A.S.: Planet. Space Sci. **59**, 402 (2011). doi:10.1016/j.pss.2011.01.006

Leonovich, A.S., Kozlov, D.A.: Earth Planets Space **65**, 369 (2013a). doi:10.5047/eps.2012.07.002

Leonovich, A.S., Kozlov, D.A.: Plasma Phys. Control. Fusion **55**(8), 085013 (2013b). doi:10.1088/0741-3335/55/8/085013

Leonovich, A.S., Mazur, V.A.: Planet. Space Sci. **37**, 1109 (1989). doi:10.1016/0032-0633(89)90082-2

Leonovich, A.S., Mazur, V.A.: Planet. Space Sci. **41**, 697 (1993). doi:10.1016/0032-0633(93)90055-7
Leonovich, A.S., Mazur, V.A.: Planet. Space Sci. **43**, 885 (1995). doi:10.1016/0032-0633(94)00207-8
Leonovich, A.S., Mazur, V.A.: Ann. Geophys. **14**, 545 (1996). doi:10.1007/s00585-996-0545-1
Leonovich, A.S., Mazur, V.A., Senatorov, V.N.: Issled. Geomagn. Aèron. Fiz. Solnca **66**, 3 (1983)
Leonovich, A.S., Mishin, V.V., Cao, J.B.: Ann. Geophys. **21**, 1083 (2003). doi:10.5194/angeo-21-1083-2003
Liu, W.W.: J. Geophys. Res. **102**, 4927 (1997). doi:10.1029/96JA03561
Mager, P.N., Klimushkin, D.Y.: Ann. Geophys. **23**, 3775 (2005). doi:10.5194/angeo-23-3775-2005
Mazur, V.A., Chuiko, D.A.: Plasma Phys. Rep. **37**, 913 (2011). doi:10.1134/S1063780X11090121
Mazur, N.G., Fedorov, E.N., Pilipenko, V.A.: Geomagn. Aeron. **52**, 603 (2012)
Mazur, N.G., Fedorov, E.N., Pilipenko, V.A.: Cosm. Res. **52**, 187 (2014)
McKenzie, J.F.: Planet. Space Sci. **18**, 1 (1970). doi:10.1016/0032-0633(70)90063-2
Ohtani, S., Miura, A., Tamao, T.: Planet. Space Sci. **37**, 567 (1989). doi:10.1016/0032-0633(89)90097-4
Parnowski, A.S.: Ann. Geophys. **25**, 1391 (2007). doi:10.5194/angeo-25-1391-2007
Rankin, R., Fenrich, F., Tikhonchuk, V.T.: Geophys. Res. Lett. **27**, 3265 (2000). doi:10.1029/2000GL000029
Southwood, D.J.: Planet. Space Sci. **22**, 483 (1974). doi:10.1016/0032-0633(74)90078-6
Southwood, D.J., Saunders, M.A.: Planet. Space Sci. **33**, 127 (1985). doi:10.1016/0032-0633(85)90149-7
Tamao, T.: Tohoku Geophys. J. **17**, 43 (1965)
Walker, A.D.M.: J. Geophys. Res. **92**, 10039 (1987). doi:10.1029/JA092iA09p10039
Walker, A.D.M., Pekrides, H.: J. Geophys. Res. **101**, 27133 (1996). doi:10.1029/96JA02701
Yumoto, K.: Planet. Space Sci. **33**, 1029 (1985). doi:10.1016/0032-0633(85)90021-2